Kinematic modelling of a 3-axis NC machine tool in linear and circular interpolation

Xavier Pessoles, Yann Landon and Walter Rubio

Université de Toulouse; INSA, UPS, Mines Albi, ISAE; ICA (Institut Clément Ader);

135, avenue de Rangueil, F-31077 Toulouse, France

Tel.: +33-(0)5-61558176

pessoles@lgmt.ups-tlse.fr

Abstract

Machining time is a major performance criterion when it comes to high speed machining. CAM software can help in estimating that time for a given strategy. But in practice, CAM programmed feed rates are rarely achieved, especially where complex surface finishing is concerned. This means that machining time forecasts are often more than one step removed from reality. The reason behind this is that CAM routines do not take either the dynamic performances of the machines or their specific machining tolerances into account. The present article seeks to improve simulation of high speed NC machine dynamic behaviour and machining time prediction, offering two models. The first contributes through enhanced simulation of 3-axis paths in linear and circular interpolation, taking high speed machine accelerations and jerks into account. The second model allows transition passages between blocks to be integrated in the simulation by adding in a polynomial transition path that caters for the true machining environment tolerances. Models are based on respect for path monitoring. Experimental validation shows the contribution of polynomial modelling of the transition passage due to the absence of a leap in acceleration. Simulation error on the machining time prediction remains below 1%.

Keywords

High speed machining; Linear interpolation; Circular interpolation; Polynomial transition

Nomenclature

Kinematic and dynamic parameters

$\overrightarrow{J}$	jerk vector
$\overrightarrow{A}$	acceleration vector
$\overrightarrow{V}$	feed rate vector
$\overrightarrow{X}$	position vector
$J_{max,i}$	maximum jerk limited by machine dynamics on the axis i
$A_{max,i}$	maximum acceleration limited by the machine dynamics on the axis i
$A_{0,i}$, $V_{0,i}$, $X_{0,i}$	acceleration, feed rate and initial position on the axis i
V_F	programmed feed rate
V_F'	feed rate reached if V_F is not achieved
$V_{c,i}$	feed rate set on the axis i
V_{In}	feed rate of entry into a block
V_{Out}	feed rate exiting a block
V_{Out}'	feed rate exiting a block if V_{Out} is not reached
V_{disc}	maximum feed rate for entering a discontinuity
V_j	feed rate entering a discontinuity limited by jerk
V_a	feed rate entering a discontinuity limited by acceleration
τ_i	duration of phase i ($\tau_i = T_i - T_{i-1}$)

Circular transitions in linear interpolation

A, O, B	theoretical programmed path
A, Q, B	path described by the machine
TIT, tol_x, tol_y	method to define point Q in accordance with the programming method
R	radius of the arc inserted on transition
l_1, l_2	length covered before and after the transition
β	angle formed by segments $[AO]$ and $[OB]$
a_c, j_t	normal acceleration and tangential jerk in steady state

Circular transitions in circular interpolation

R_1, R_2	radii of circles before and after a circle - circle transition

Parameters used in circular interpolation

O	centre of circle
R	radius of circle
$P(t)$	current point
α	angle covered by the circle arc
$\theta(t)$	current angle
J_i	curvilinear jerk limited by the axis i
J_C	curvilinear jerk
A_i	curvilinear acceleration limited by the axis i
A_C	curvilinear acceleration

Polynomial transitions in linear interpolation

$\mathcal{R}$	frame $\left(O, \overrightarrow{X}, \overrightarrow{Y}, \overrightarrow{Z}\right)$
A, O, B	programmed theoretical path
(x_A, y_A, z_A)	coordinates of $\overrightarrow{OA}$ in the frame $\mathcal{R}$
(x_B, y_B, z_B)	coordinates of $\overrightarrow{OB}$ in the frame $\mathcal{R}$
M	point of entry into the discontinuity
N	point of exit from the discontinuity
Q	effective point of passage in the discontinuity
T	time of passage in the discontinuity
L	distance OM
$P(t)$	current point
ϕ_i, θ_i	spherical coordinates of the point i
tol_x, tol_y, tol_z	tolerance of position on the axes
V_M, V_N	feed rates for entry on M and exit on N

1   Introduction

High speed machining centres allow for extremely high feed rates to be programmed. However, when machining molds or dies, dynamic performances of the machines do not always allow such feed rates to be reached. Indeed, according to the quality sought, the segments making up the machining path are often extremely short and in such conditions the feed rate reached by the machine will then be limited by the NC interpolation time or even the capabilities in jerk or acceleration of the axes [1], [2]. The feed rate will then not be constant, leading to considerably lower productivity, a variation in tangential cutting forces and impaired quality [3]. Many publications relating to the search to reduce the number of feed rate changes base their research on the use of NURBS interpolations. [4] [5] [6] or B-spline [7]. However, in the industrial world, linear and circular interpolation remain the most frequently used methods on many workpieces. Precise simulation of this type of movement is therefore essential.

The aim of this work is therefore to propose a comprehensive model intended to simulate the position, feed rate, acceleration and jerk in 3-axis linear and circular interpolation taking the machine/NC combination parameters into account.

At present, NC machine manufacturers [8] propose a displacement law on the axes in trapezoid acceleration. This type of command has been studied in the literature by a number of authors writing on uniaxial paths with null initial and final feed rates [9] [10]. This movement involves 7 phases (figure 1):

- On phase 1,

$$\forall t \in [T_0, T_1] \begin{cases} J_i(t) &= J_{max,i} \\ A_i(t) &= A_{0,i} + J_{max,i}(t - T_0) \\ V_i(t) &= V_{0,i} + A_{0,i}(t - T_0) \\ &\quad + \frac{1}{2} J_{max,i}(t - T_0)^2 \\ X_i(t) &= X_{0,i} + V_{0,i}(t - T_0) + \\ &\quad \frac{1}{2} A_{0,i}(t - T_0)^2 + \\ &\quad \frac{1}{6} J_{max,i}(t - T_0)^3 \end{cases} \tag{1}$$

- On phase 2,

$$\forall t \in [T_1, T_2] \begin{cases} J_i(t) &= 0 \\ A_i(t) &= A_{max,i} \\ V_i(t) &= V_i(T_1) + A_{max,i}(t - T_1) \\ X_i(t) &= X_i(T_1) + V_i(T_1)(t - T_1) \\ &\quad + \frac{1}{2} A_{max,i}(t - T_1)^2 \end{cases} \tag{2}$$

- On phase 3,

$$\forall t \in [T_2, T_3] \begin{cases} J_i(t) &= -J_{max,i} \\ A_i(t) &= A_i(T_2) - J_{max,i}(t - T_2) \\ V_i(t) &= V_i(T_2) + A_i(T_2)(t - T_2) \\ &\quad - \frac{1}{2} J_{max,i}(t - T_2)^2 \\ X_i(t) &= X_i(T_2) + V_i(T_2)(t - T_2) + \\ &\quad \frac{1}{2} A_i(T_2)(t - T_2)^2 \\ &\quad - \frac{1}{6} J_{max,i}(t - T_2)^3 \end{cases} \tag{3}$$

- On phase 4,

$$\forall t \in [T_3, T_4] \begin{cases} J_i(t) &= 0 \\ A_i(t) &= 0 \\ V_i(t) &= V_{c,i} \\ X_i(t) &= X_i(T_3) + V_{c,i}(t - T_3) \end{cases} \tag{4}$$

- On phase 5,

$$\forall t \in [T_4, T_5] \begin{cases} J_i(t) &= -J_{max,i} \\ A_i(t) &= A_i(T_4) - J_{max,i}(t - T_4) \\ V_i(t) &= V_i(T_4) + A_i(T_4)(t - T_4) \\ &\quad - \frac{1}{2} J_{max,i}(t - T_4)^2 \\ X_i(t) &= X_i(T_4) + V_i(T_4)(t - T_4) \\ &\quad + \frac{1}{2} A_i(T_4)(t - T_4)^2 \\ &\quad - \frac{1}{6} J_{max,i}(t - T_4)^3 \end{cases} \tag{5}$$
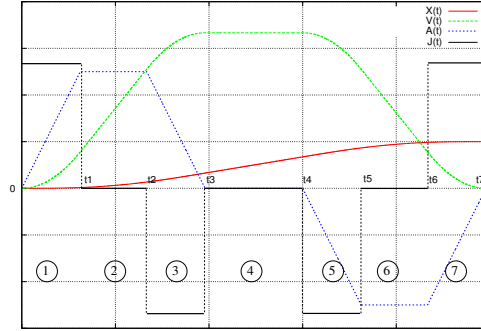
- On phase 6,

$$\forall t \in [T_5, T_6] \begin{cases} J_i(t) &= 0 \\ A_i(t) &= -A_{max,i} \\ V_i(t) &= V_i(T_5) - A_{max,i}(t - T_5) \\ X_i(t) &= X_i(T_5) + V_i(T_5)(t - T_5) \\ &\quad -\frac{1}{2}A_{max,i}(t - T_5)^2 \end{cases} \tag{6}$$

- On phase 7,

$$\forall t \in [T_6, T_7] \begin{cases} J_i(t) &= J_{max,i} \\ A_i(t) &= A_i(T_6) + J_{max,i}(t - T_6) \\ V_i(t) &= V_i(T_6) + A_i(T_6)(t - T_6) \\ &\quad +\frac{1}{2}J_{max,i}(t - T_6)^2 \\ X_i(t) &= X_i(T_6) + V_i(T_6)(t - T_6) \\ &\quad +\frac{1}{2}A_i(T_6)(t - T_6)^2 \\ &\quad +\frac{1}{6}J_{max,i}(t - T_6)^3 \end{cases} \tag{7}$$

Figure 1: Control law for a translation axis

Acceleration starts by increasing up to its maximum value $A_{max,i}$. The slope for this acceleration is called jerk. This is noted $J_{max,i}$ (phase 1). An acceleration level is then reached with value $A_{max,i}$ (phase 2). This then diminishes down to zero (phase 3). During the fourth stage, acceleration is null and the feed rate attained is equal to the programmed feed rate. Phases 5, 6 and 7 are symmetrical with phases 3, 2 and 1. Time resolution of this system of equations allows the times for each of the phases to be calculated readily (section 2.1). Parameters $A_{max,i}$ and $J_{max,i}$ are specific to the dynamics of the machine used.

In practice, the blocks follow on from each other and the feed rates at the start and end of the blocks are rarely null. Furthermore, according to the length of the segment and the feed rate to be reached, maximum acceleration or the programmed feed rate are not always reached. Thus, segments are often crossed in which some of the seven phases do not exist. This general case is rarely addressed [9] [11]. Modelling of the machine's behaviour taking these aspects into account is proposed in section 2.

In the case of 3-axis machining, the path of a segment is covered simultaneously on 3 axes. Take, for example, the case of a block with displacement on $\overrightarrow{X}$ and $\overrightarrow{Y}$. To ensure the quality of the machined workpiece, the path actually followed needs to be monitored in relation to the programmed path. To do

6

so, synchronization of the axes is needed. Indeed, both axes must reach the final position at the same instant. Thus, on 3 axes, a feed rate, an acceleration and a maximum jerk have to be calculated for each of the axes as a function of the slowest axis [12]. Using the model in 7 phases, the same time for each of the phases will be obtained on each of the axes, allowing the path to be followed.

Circular interpolation is also widely used. However, as far as can be ascertained, there are no publications covering changes in feed rate on a circle while also ensuring monitoring of the path to be followed. Modelling of such a case will be presented in section 2.

Moreover, a machining operation can be broken down into a multitude of linear or circular blocks. This thus poses the problem of the crossing of transitions between discontinuous blocks tangent to each other. From a purely kinematic point of view, the exact passage by the programmed points requires precise arrest of the machine at the end of each block. This behaviour is not permitted in practice as it implies repeatedly slowing down and thus a loss in productivity. In addition, the jerks are prejudicial to the quality of the workpieces manufactured as well as the lifetime of the cutting tools used. Thus, in numerical commands, there is a tolerance on pursuit of the path, figure 2. For a programmed path $A - O - B$, the machine will cover the path $A - Q - B$. This point Q can be defined in a number of ways: by the distance TIT, tolerances tol_x and tol_y on the axes and the distances d_1 or d_2.

Figure 2: Model of circular pass for a discontinuity at a tangent
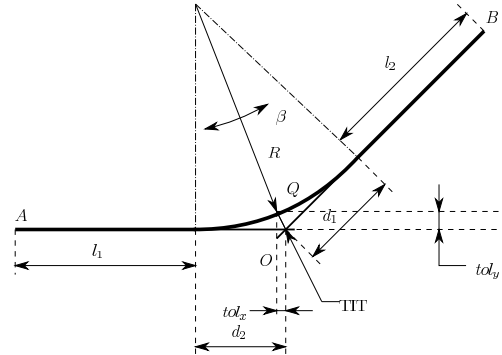
In the literature, a circle arc is used to model this transition [14]. Radius R of this circle arc is calculated in relation to the tolerance permitted by the NC and lengths l_1 and l_2 of the blocks before and after the discontinuity:

$$R = \min \left(TIT \frac{\cos\left(\frac{\beta}{2}\right)}{1 - \cos\left(\frac{\beta}{2}\right)}, \frac{l}{\sin\left(\frac{\beta}{2}\right)} - TIT \right) \tag{8}$$

where $l = \min(l_1, l_2)$.

From a kinematic point of view, the course of a circle at constant feed rate V runs at constant centripetal acceleration $a_c = \frac{V_F^2}{R}$. Deriving this acceleration, a constant tangential jerk $j_t = \frac{V^3}{R^2}$ is also obtained. As this acceleration a_c and jerk j_t are limited on the machine by maximum values $A_{max,i}$ and $J_{max,i}$, for a given radius, the feed rate in the discontinuity will thus be limited:

$$V_{disc} = \min \left(V_F, V_a = \sqrt{A_{max,i}R}, V_j = \sqrt[3]{J_{max,i}R^2} \right) \tag{9}$$

7

This modelling allows the maximum speed of passage to be expressed as a discontinuity. However, it pre-supposes a jump in acceleration: at constant feed rate on segment [AO] acceleration is null (phase 4) while at constant speed on a circle, the projection of the acceleration vector on the axes can reach V_F^2/R. This leap in acceleration on crossing the transition is not observed in practice. Thus, a circular model cannot be used to simulate precisely the position, feed rate, acceleration and jerk along the discontinuity, even if it gives a good approximation of the drop in feed rate. In part 3, a polynomial form of modelling for transitions between non-tangent segments will be presented.

In circular interpolation, the transitions between the circles of different radii need to be modelled. In this case, the same type of limitation arises: two tangent circles with different radii are discontinuous in curvature. On crossing the discontinuity, there will thus be a jump in acceleration. Pateloup [15] proposes a model to determine the minimum feed rate needed to cross the discontinuity taking into account the jerk j, the radii R_1 and R_2 of the two circular portions, and the interpolation time δ_t of the machine:

$$V_{disc} = \sqrt{\frac{R_1 R_2}{|R_1 - R_2|\,\delta_t j}} \tag{10}$$

This model is also used to cross a transition between a segment of a straight line and a circle arc when they are tangent. The model is again taken up in the algorithm proposed by Tapie [1] to calculate the entry rate into this type of discontinuity. This method for crossing discontinuities will be validated in section 4.

With the aim of simulating a complete path (path including blocks and transitions), Lavernhe [12] proposes a method allowing the machine's dynamic behaviour to be computed using a formalism with inverse time. Integration of the NC cycle time in this method allows it to predict the control jerk value to be predicted for each of the periods. From this are deduced the plots for acceleration and feed rate. Furthermore, his model takes the predictive functions available on NCs into account. The model for crossing of discontinuities in tangency is that described previously (circle arc).

Another solution is to identify the servo-system model for the machine/NC combination [13]. This approach appears difficult to implement given the lack of data provided by NC manufacturers. Indeed, to apply this approach would require precise knowledge of the slaving flow diagrams for the axes and especially the various correctors used. Where appropriate, tests need to be conducted to identify the transfer function parameters.

Finally, a third method involves modelling directly the laws described in the previous sections. The difficulty in implementing these models lies in calculating for each block the time for each acceleration phase as well as the jerk on each axis. Integration of anticipation is no easy matter.

To sum up, the paths of linear blocks are clearly described in the literature. However, the general case (path of a segment at non-null initial and final feed rates) is not studied. Furthermore, no information is to be found on the path of circular blocks. With respect to discontinuities in tangency, the model for passage in a circle arc allows the feed rate on crossing the discontinuity to be quantified but does not enable laws for feed rates and accelerations to be modelled. The idea is to propose algorithms that, on 3 axes, show how to go from a feed rate on block entry V_{In} to a feed rate on block exit V_{Out} while attempting to reach the programmed rate V_F both in linear interpolation (section 2.1) and circular interpolation (section 2.3).

8

A model is then proposed for passage into discontinuities in tangency between two straight lines (section 3). Finally, tests validating the simulator are presented.

2 Modelling NC behaviour in linear and circular interpolation

In this section, the laws for displacements, feed rates, accelerations and jerks to cover a uniaxial segment from a feed rate V_{In} to a feed rate V_{Out} passing through a feed rate V_F are modelled. Passage in the case of a 3-axis segment is then studied. The results are then adapted to circular interpolation.

2.1 Modelling uniaxial linear segments in the general case

In the general case of a toolpath for a segment in 3-axis machining, the feed rates at entry, middle and exit of a segment will not be identical. In addition, according to the jumps in feed rate to be crossed and the length of the displacement to be made, the feed rate will not necessarily be reached. As a result, resolution of equations 1 to 7 allows all existing cases to be identified (figure 3 and appendices). Thus, for L, V_F, V_{In} and V_{Out} given, it can be determined whether V_{out} and/or V_F will be reached going through $A_{max,i}$ or not. This means the duration for each of the phases can be known. The contour for jerk, acceleration, feed rate and position on one axis can thus be retraced.

Figure 3: Set of cases of resolution
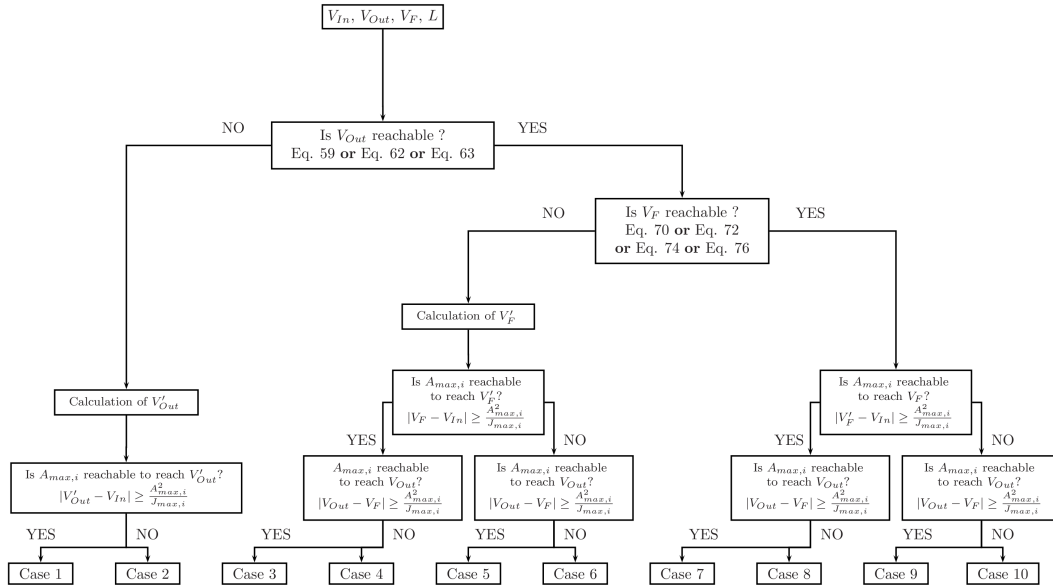
2.2 Passage to 3 axes

The algorithm given in the previous section is valid on a uniaxial displacement. In this case, values $A_{max,i}$ and $J_{max,i}$ will derive from the machine characteristics. On 3 axes, synchronization will be

9

needed. This means that the times for each of the 7 phases are identical on all axes. As a result, for a given displacement at a given programmed feed rate, the NC will recalculate a set feed rate, acceleration and jerk for each of the axes.

The modelling method followed is thus as follows: for a given segment, the displacement to be made on each of the axes is calculated. Using the results of the previous section with maximum acceleration and maximum jerk, it will thus be possible to determine which of the 3 axes will be the slowest. Then, using the results Lavernhe offers [12], feed rates V_i, accelerations A_i and jerks J_i on the axes limited i can thus be calculated as a function of the distance L_{lim} to be covered on the limiting axis and distances L_i to be covered on the limited axes:

$$V_i = \frac{L_i}{L_{lim}} V_F \quad A_i = \frac{L_i}{L_{lim}} A_{max,i} \quad J_i = \frac{L_i}{L_{lim}} J_{max,i} \tag{11}$$

All the elements used to simulate tool paths in 3-axis linear interpolation have thus been presented. In what follows, the case of circular interpolation will be studied.

2.3 Modelling tool paths defined by circle arcs

As has been seen, few data are given as to simulation of displacements on a circle. The problem involves understanding how the axes of the NC behave to follow a circular path and especially how decelerations and accelerations are made when following a circle. To this purpose, the laws governing a circular movement can be stated.

Let P be a point moving over a circle arc of angle θ, centre O and radius R in the frame $(\vec{e_r}, \vec{e_\alpha}, \vec{e_z})$ (figure 4).

Figure 4: Parametrization for a circular path
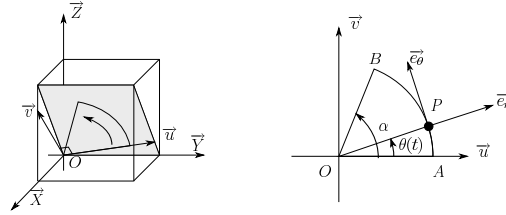
This gives:

$$\overrightarrow{OP} = R\vec{e_r} \tag{12}$$

Note θ the angular law such that $\forall t \in [0, T]$, $\theta(0) = 0$ and $\theta(T) = \alpha$. The feed rate, acceleration and jerk vectors can thus be expressed as follows:

$$\frac{d\overrightarrow{OP}}{dt} = R\frac{d\theta}{dt}\vec{e_\theta} \tag{13}$$

$$\frac{d^2\overrightarrow{OP}}{dt^2} = R\frac{d^2\theta}{dt^2}\vec{e_\theta} - R\left(\frac{d\theta}{dt}\right)^2\vec{e_r} \tag{14}$$

$$\frac{d^3\overrightarrow{OP}}{dt^3} = R\left(\frac{d^3\theta}{dt^3} - \left(\frac{d\theta}{dt}\right)^3\right)\vec{e_\theta} - 3R\frac{d^2\theta}{dt^2}\frac{d\theta}{dt}\vec{e_r} \tag{15}$$

10

When the set feed rate is reached, $d\theta(t)/dt = V_F/R$. Nevertheless, the angle law $\theta(t)$ is unknown on passage from null feed rate to the programmed feed rate. As a result, using a law in 7 phases is proposed, like that considered in section 2.1. In these conditions the jerk effect no longer corresponds to a jerk by axis, but a "curvilinear" jerk taking into account the influence of 2 or 3 axes along the plane in which the circle is made. This jerk is thus the result of several contributing axes. This means the tool path has to be expressed as a projection on the machine's axes of translation. This is done through two moves in frames.

Let $\mathcal{M}_1$ and $\mathcal{M}_2$ be the respective matrices for passage of the frame $(\overrightarrow{u}, \overrightarrow{v}, \overrightarrow{w})$ towards frame $(\overrightarrow{x}, \overrightarrow{y}, \overrightarrow{z})$ and the frame $(\overrightarrow{e_R}, \overrightarrow{e_\theta}, \overrightarrow{e_z})$ towards frame $(\overrightarrow{u}, \overrightarrow{v}, \overrightarrow{w})$.

$\mathcal{M}$ is noted as the matrix for passage of the frame $(\overrightarrow{x}, \overrightarrow{y}, \overrightarrow{z})$ to frame $(\overrightarrow{e_R}, \overrightarrow{e_\theta}, \overrightarrow{e_z})$:

$$\mathcal{M} = (\mathcal{M}_1\mathcal{M}_2)^{-1} \tag{16}$$

2.4   Calculation of jerk and curvilinear acceleration

Curvilinear jerk and curvilinear acceleration do not form part of the machine parameters, but they are the result of the contribution made by accelerations and jerks for each axis in movement. According to the zone in which the circle is completed, one or other of the axes will be limiting.

These parameters are calculated at the start and the end of movement as that is where they are most significant. Indeed, for the path of a circle arc, one needs to switch from a null normal acceleration to a normal acceleration equivalent to V_F^2/R at the start and at the end of the path, which would require an infinite jerk at the start or the end of the path. As this can only be considered on certain types of machining centres, the maximum jerk that can be reached at the start and end of the path in consideration of the characteristics of the axes is thus calculated.

Consider a circle arc made in the frame $(\overrightarrow{u}, \overrightarrow{v}, \overrightarrow{w})$ from an angle $\theta(0) = 0$ to an angle $\theta(T) = \alpha$, T being the overall duration of the path. In this general case, the matrix $\mathcal{M}$ is a matrix for rotation of the orthonormed frame $(\overrightarrow{e_R}, \overrightarrow{e_\theta}, \overrightarrow{e_z})$ to the orthonormed frame $(\overrightarrow{x}, \overrightarrow{y}, \overrightarrow{z})$. This matrix is thus orthogonal and can be inverted. Note (u_x, u_y, u_z), (v_x, v_y, v_z), (w_x, w_y, w_z) the coordinates of the vectors $\overrightarrow{u}$, $\overrightarrow{v}$, $\overrightarrow{w}$ in the frame $(\overrightarrow{x}, \overrightarrow{y}, \overrightarrow{z})$.

Using a model in 7 phases for angular acceleration and assuming initial acceleration to be null, the following is obtained on the first phase, $\forall t \in [0, T_1]$:

$$\begin{cases} \frac{d^3\theta}{dt^3}(t) = J_c \\ \frac{d^2\theta}{dt^2}(t) = J_c t \\ \frac{d\theta}{dt}(t) = \dot{\theta}_{In} + \frac{1}{2}J_c t^2 \\ \theta(t) = \dot{\theta}_{In} t + \frac{1}{6}J_c t^3 \end{cases} \tag{17}$$

with J_c the curvilinear jerk. Carrying over equation 17 into equation 15 on $t = 0$ and projecting onto the machine axes, the following is obtained:

$$\frac{d^3\overrightarrow{OP}}{dt^3} = R\left(J_c - \dot{\theta}_{In}^3\right)\overrightarrow{e_\theta} = \begin{pmatrix} R\left(J_c - \dot{\theta}_{In}^3\right)v_x \\ R\left(J_c - \dot{\theta}_{In}^3\right)v_x \\ R\left(J_c - \dot{\theta}_{In}^3\right)v_x \end{pmatrix}_{(\overrightarrow{x},\overrightarrow{y},\overrightarrow{z})} \tag{18}$$

Jerk is limited on each of the axes and curvilinear jerk will depend on 2 or even 3 axes. The latter will thus depend on the axis that will be limiting. The following will therefore obtain:

$$J_1 = \frac{J_{max,x}}{Rv_x} + \dot{\theta}_{In}^3 \quad J_2 = \frac{J_{max,y}}{Rv_y} + \dot{\theta}_{In}^3 \quad J_3 = \frac{J_{max,z}}{Rv_z} + \dot{\theta}_{In}^3 \tag{19}$$

Similarly, J_4, J_5, J_6 are calculated at the end of movement to obtain:

$$J_c = \min_{i \in [1,6]} (J_i) \tag{20}$$

Curvilinear acceleration A_c can now be calculated. Noting θ_1, the position reached at the end of phase 1 and $\dot{\theta}_1$ the feed rate reached at the end of phase 1, the following will obtain in phase 2, $\forall t \in [T_1, T_2]$:

$$\begin{cases} \frac{d^3\theta}{dt^3}(t) = 0 \\ \frac{d^2\theta}{dt^2}(t) = A_c \\ \frac{d\theta}{dt}(t) = \dot{\theta}_1 + A_c t \\ \theta(t) = \theta_1 + \dot{\theta}_1 t + \frac{1}{2}A_c t^2 \end{cases} \tag{21}$$

Carrying over equation 21 into equation 14, this gives $t = T_1$:

$$\begin{aligned} \frac{d^2\overrightarrow{OP}}{dt^2} &= RA_c\overrightarrow{e_\theta} - R\dot{\theta}_1^2\overrightarrow{e_r} \\ &= \Big(-(u_x\cos\theta_1 + v_x\sin\theta_1)R\dot{\theta}_1^2 \\ &\quad + (u_y\cos\theta_1 + v_y\sin\theta_1)RA_c\Big) \cdot \overrightarrow{x} \\ &\quad + \Big(-(-u_x\sin\theta_1 + v_x\cos\theta_1)R\dot{\theta}_1^2 \\ &\quad + (-u_y\sin\theta_1 + v_y\cos\theta_1)RA_c\Big) \cdot \overrightarrow{y} \\ &\quad + \Big(-w_x R\dot{\theta}_1^2 + w_y RA_c\Big) \cdot \overrightarrow{z} \end{aligned} \tag{22}$$

Thus:

$$\begin{aligned} A_1 &= \frac{A_{max,x} + (u_x\cos\theta + v_x\sin\theta)R\dot{\theta}_1^2}{(u_y\cos\theta + v_y\sin\theta)R} \\ A_2 &= \frac{A_{max,y} + (-u_x\sin\theta_1 + v_x\cos\theta_1)R\dot{\theta}_1^2}{(-u_y\sin\theta_1 + v_y\cos\theta_1)R} \\ A_3 &= \frac{A_{max,z} + w_x R\dot{\theta}_1^2}{w_y R} \end{aligned} \tag{23}$$

The same method is adopted for the deceleration phase, giving:

$$A_c = \min_{i \in [1,6]} (A_i) \tag{24}$$

To conclude, in the modelling proposed in circular interpolation, the angular law follows a movement in seven phases, with maximum jerk being the calculated value J_c and maximum acceleration being the calculated value A_c. Knowing all the parameters of a circle arc (point of departure, point of arrival, radius, etc.), the machine's dynamic behaviour can be simulated throughout the circular path.

This part allows the laws of position, feed rate, acceleration and jerk on unique blocks in circular and linear interpolation to be simulated. What remains is to model the junctions between blocks. It has already been shown that the model for transition between two tangent paths functions. The following part of the article will cover how to model the passage between two linear segments.

3   Modelling of the transition between two rectilinear blocks

In the literature, transitions between two segments are always modelled by circle arcs, though this does not seem to match the real behaviour of the machine. Knowing that NCs are capable of describing polynomials of degree 5, it is suggested that they be used to model discontinuities in tangency. This model should allow a criterion for feed rate for entry into the discontinuity to be defined as also the contour for position, feed rate, acceleration and jerk in the discontinuity.

3.1   Notations and hypotheses

Consider the paths of two consecutive non-aligned segments AO and OB (figure 5).

Figure 5: Parametrization of passage of discontinuity
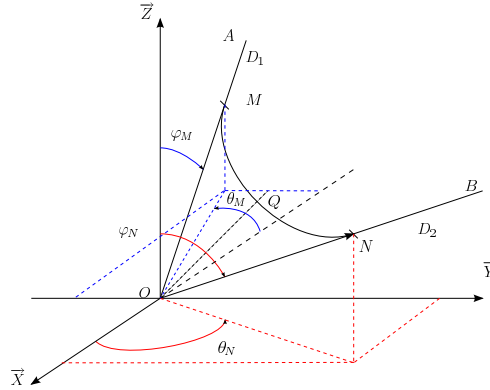
The points M and N can be expressed as follows in this frame:

$$
\overrightarrow{OM} = \begin{pmatrix} L\sin\varphi_M\cos\theta_M \\ L\sin\varphi_M\sin\theta_M \\ L\cos\varphi_M \end{pmatrix}_{\mathcal{R}} = L\overrightarrow{u}
$$
$$
\overrightarrow{ON} = \begin{pmatrix} L\sin\varphi_N\cos\theta_N \\ L\sin\varphi_N\sin\theta_N \\ L\cos\varphi_N \end{pmatrix}_{\mathcal{R}} = L\overrightarrow{v}
\tag{25}
$$

These notations allow the working assumptions to be determined. Firstly, it shall be considered that:

$$
||\overrightarrow{OM}|| = ||\overrightarrow{ON}|| = L
\tag{26}
$$

Then, considering the problem to be symmetrical, this gives:

$$\overrightarrow{OQ} = ||\overrightarrow{OQ}|| \cdot \frac{\overrightarrow{u} + \overrightarrow{v}}{||\overrightarrow{u} + \overrightarrow{v}||} = ||\overrightarrow{OQ}|| \cdot \overrightarrow{w} = \begin{pmatrix} Q_x \\ Q_y \\ Q_z \end{pmatrix}_{\mathcal{R}} \tag{27}$$

The coordinates of point Q can then be expressed in the frame $\mathcal{R}$:

$$\overrightarrow{OQ} = ||\overrightarrow{OQ}|| \cdot \begin{pmatrix} \sin\varphi_Q \cos\theta_Q \\ \sin\varphi_Q \sin\theta_Q \\ \cos\varphi_Q \end{pmatrix}_{\mathcal{R}}$$

$$\begin{cases} \varphi_Q = \arccos \frac{w_z}{\sqrt{w_x^2 + w_y^2 + w_z^2}} \\ \text{Si } w_x \geq 0\,, \ \theta_Q = \arcsin \frac{w_y}{\sqrt{w_x^2 + w_y^2}} \\ \text{Si } w_x < 0\,, \ \theta_Q = \pi - \arcsin \frac{w_y}{\sqrt{w_x^2 + w_y^2}} \end{cases} \tag{28}$$

The direction of the vector $\overrightarrow{OQ}$ is thus fully determined by the vectors $\overrightarrow{u}$ and $\overrightarrow{v}$. Its norm now needs to be determined. This is done by the tolerance granted the machine on passage of the discontinuity (section 1 and figure 1). In this instance, tol_x, tol_y and tol_z denote the maximum tolerances for passage used by the NC on each of the axes $\overrightarrow{X}$, $\overrightarrow{Y}$ and $\overrightarrow{Z}$, which means that:

$$\begin{cases} \overrightarrow{OQ} \cdot \overrightarrow{X} \leq tol_x \\ \overrightarrow{OQ} \cdot \overrightarrow{Y} \leq tol_y \\ \overrightarrow{OQ} \cdot \overrightarrow{Z} \leq tol_z \end{cases} \tag{29}$$

The norm of vector $\overrightarrow{OQ}$ can thus be calculated as follows:

$$||\overrightarrow{OQ}|| = \min\left(\frac{tol_x}{|\sin\varphi_Q \cos\theta_Q|}, \frac{tol_y}{|\sin\varphi_Q \sin\theta_Q|}, \frac{tol_z}{|\cos\varphi_Q|}, \right) \tag{30}$$

Finally, due to the problem's symmetry, it can be considered that the entry feed rate in the discontinuity $||\overrightarrow{V_M}||$ and the exit feed rate $||\overrightarrow{V_N}||$ will be equal:

$$\overrightarrow{V_M} = -V_{In}\overrightarrow{u} \quad \overrightarrow{V_N} = V_{In}\overrightarrow{v} \tag{31}$$

As points A, M and O, as well as points B, N and O are aligned, angles φ_M, θ_M, φ_N and θ_N can thus be calculated:

$$\begin{cases} \varphi_M = \arccos \frac{z_A}{\sqrt{x_A^2 + y_A^2 + z_A^2}} \\ \text{Si } x_A \geq 0\,, \ \theta_M = \arcsin \frac{y_A}{\sqrt{x_A^2 + y_A^2}} \\ \text{Si } x_A < 0\,, \ \theta_M = \pi - \arcsin \frac{y_A}{\sqrt{x_A^2 + y_A^2}} \\ \varphi_N = \arccos \frac{z_B}{\sqrt{x_B^2 + y_B^2 + z_B^2}} \\ \text{Si } x_B \geq 0\,, \ \theta_N = \arcsin \frac{y_B}{\sqrt{x_B^2 + y_B^2}} \\ \text{Si } x_B < 0\,, \ \theta_N = \pi - \arcsin \frac{y_B}{\sqrt{x_B^2 + y_B^2}} \end{cases} \tag{32}$$

3.2 Formation of the equation

Using a polynomial representation, the equation for the position, feed rate, acceleration and jerk of the point P in the discontinuity thus takes the following form, $\forall t \in [0, T]$:

$$\overrightarrow{OP}(t) = \begin{bmatrix} \sum_{i=0}^{5} a_i t^i \\ \sum_{i=0}^{5} b_i t^i \\ \sum_{i=0}^{5} c_i t^i \end{bmatrix} \tag{33}$$

$$\frac{d\overrightarrow{OP}(t)}{dt} = \begin{bmatrix} \sum_{i=1}^{5} i a_i t^{i-1} \\ \sum_{i=1}^{5} i b_i t^{i-1} \\ \sum_{i=1}^{5} i c_i t^{i-1} \end{bmatrix} \tag{34}$$

$$\frac{d^2\overrightarrow{OP}(t)}{dt^2} = \begin{bmatrix} \sum_{i=2}^{5} \frac{i!}{(i-2)!} a_i t^{i-2} \\ \sum_{i=2}^{5} \frac{i!}{(i-2)!} b_i t^{i-2} \\ \sum_{i=2}^{5} \frac{i!}{(i-2)!} c_i t^{i-2} \end{bmatrix} \tag{35}$$

$$\frac{d^3\overrightarrow{OP}(t)}{dt^2} = \begin{bmatrix} \sum_{i=3}^{5} \frac{i!}{(i-3)!} a_i t^{i-3} \\ \sum_{i=3}^{5} \frac{i!}{(i-3)!} b_i t^{i-3} \\ \sum_{i=3}^{5} \frac{i!}{(i-3)!} c_i t^{i-3} \end{bmatrix} \tag{36}$$

3.3 Boundary conditions

In order to resolve this system, eight boundary conditions are used:

$$\overrightarrow{OP}(0) = \overrightarrow{OM} \tag{37}$$

$$\overrightarrow{OP}(T) = \overrightarrow{ON} \tag{38}$$

$$\overrightarrow{OP}\left(\frac{T}{2}\right) = \overrightarrow{OQ} \tag{39}$$

$$\overrightarrow{V}(0) = \overrightarrow{V_M} = -V_{In}\overrightarrow{u} \tag{40}$$

$$\overrightarrow{V}(T) = \overrightarrow{V_N} = V_{In}\overrightarrow{v} \tag{41}$$

$$\overrightarrow{A}(0) = \overrightarrow{0} \tag{42}$$

$$\overrightarrow{A}(T) = \overrightarrow{0} \tag{43}$$

$$\overrightarrow{J}\left(\frac{T}{2}\right) = \overrightarrow{0} \tag{44}$$

Equations 37 and 38 translate entry into the discontinuity. Equation 39 translates the problem's symmetry, meaning that the point parametrized by tolerances of passage is reached half way through the time of the path. Considering that acceleration is null at entry and exit of the discontinuity, equations 42 and 43 are obtained. To conclude, equation 44 translates symmetry of the acceleration contour.

3.4 Resolution

This thus involves resolving a system of 24 scalar equations (projection of equations 37 onto 44) whose unknowns are:

- 18 coefficients a_i, b_i, c_i of polynomials,

- the norm L of vectors $\overrightarrow{OM}$ and $\overrightarrow{ON}$,

- time T for passage of the transition.

Resolving the system gives:

$$
\begin{cases}
a_0 = \frac{16Q_x \sin\varphi_M \cos\theta_M}{3(\sin\varphi_N \cos\theta_N + \sin\varphi_M \cos\theta_M)} \\
b_0 = \frac{16Q_y \sin\varphi_M \sin\theta_M}{3(\sin\varphi_N \sin\theta_N + \sin\varphi_M \sin\theta_M)} \\
c_0 = \frac{16Q_z \cos\varphi_M}{3(\cos\varphi_N + \cos\varphi_M)}
\end{cases}
\tag{45}
$$

$$
\begin{cases}
a_1 = -V_{In} \sin\varphi_M \cos\theta_M \\
b_1 = -V_{In} \sin\varphi_M \sin\theta_M \\
c_1 = -V_{In} \cos\varphi_M
\end{cases}
\tag{46}
$$

$$
\begin{cases}
a_2 = 0 \\
b_2 = 0 \\
c_2 = 0
\end{cases}
\tag{47}
$$

$$
\begin{cases}
a_3 = \frac{9(\sin\varphi_N \cos\theta_N + \sin\varphi_M \cos\theta_M)^3 V_{In}^3}{1024 Q_x^2} \\
b_3 = \frac{9(\sin\varphi_N \sin\theta_N + \sin\varphi_M \sin\theta_M)^3 V_{In}^3}{1024 Q_y^2} \\
c_3 = \frac{9(\cos\varphi_N + \cos\varphi_M)^3 V_{In}^3}{1024 Q_z^2}
\end{cases}
\tag{48}
$$

$$
\begin{cases}
a_4 = -\frac{27(\sin\varphi_N \cos\theta_N + \sin\varphi_M \cos\theta_M)^4 V_{In}^4}{65536 Q_x^3} \\
b_4 = -\frac{27(\sin\varphi_N \sin\theta_N + \sin\varphi_M \sin\theta_M)^4 V_{In}^4}{65536 Q_y^3} \\
c_4 = -\frac{27(\cos\varphi_N + \cos\varphi_M)^4 V_{In}^4}{65536 Q_z^3}
\end{cases}
\tag{49}
$$

$$
\begin{cases}
a_5 = 0 \\
b_5 = 0 \\
c_5 = 0
\end{cases}
\tag{50}
$$

$$
\overrightarrow{OP}(T) = \overrightarrow{ON} \Longleftrightarrow
$$
$$
\begin{pmatrix} T \\ T \\ T \end{pmatrix} = \begin{pmatrix} \frac{32Q_x}{3V_{In}(\sin\varphi_N \cos\theta_N + \sin\varphi_M \cos\theta_M)} \\ \frac{32Q_y}{3V_{In}(\sin\varphi_N \sin\theta_N + \sin\varphi_M \sin\theta_M)} \\ \frac{32Q_z}{3V_{In}(\cos\varphi_N + \cos\varphi_M)} \end{pmatrix}
\tag{51}
$$

$$
\overrightarrow{OP}\left(\frac{T}{2}\right) = \overrightarrow{OQ} \Longleftrightarrow
$$
$$
\begin{pmatrix} L \\ L \\ L \end{pmatrix} = \begin{pmatrix} \frac{16Q_x}{3(\sin\varphi_N \cos\theta_N + \sin\varphi_M \cos\theta_M)} \\ \frac{16Q_y}{3(\sin\varphi_N \sin\theta_N + \sin\varphi_M \sin\theta_M)} \\ \frac{16Q_z}{3(\cos\varphi_N + \cos\varphi_M)} \end{pmatrix}
\tag{52}
$$

Due to the relation between Q_x, Q_y and Q_z, the 3 expressions allowing L or T to be computed give the same results. With respect to the feed rate on entry of the discontinuity V_{In}, it is *ex ante* equal to the feed rate at the end of the upstream block. Nevertheless, it can perhaps be limited by maximum jerk, maximum acceleration and the length of the blocks upstream and downstream from the transition. This feed rate can now be calculated.

3.5 Feed rate on entry in the discontinuity

Expressing the problem as an equation allows the entry feed rate to be calculated when it is limited by acceleration or maximum jerk: the assumption is made that maximum jerk is at point M and that acceleration will be at its maximum at Q. Care must therefore be taken to ensure that the machine's capabilities are not exceeded at these points.

If the maximum jerk is reached on each of the axes, the equation gives:

$$\overrightarrow{J}(0) = \overrightarrow{J_{max,i}} \iff 6 \begin{pmatrix} a_3 \\ b_3 \\ c_3 \end{pmatrix} = \begin{pmatrix} J_{max,x} \\ J_{max,y} \\ J_{max,z} \end{pmatrix} \tag{53}$$

According to the case, resolution of this system allows the entry rate limited by an axial jerk to be determined using the results given by equation 48:

$$V_{lim,j} \quad = \quad \frac{8}{3|\sin\varphi_N\cos\theta_N + \sin\varphi_M\cos\theta_M|} \cdot \min\left(\sqrt[3]{Q_x^2 J_{max,x}}, \sqrt[3]{Q_y^2 J_{max,y}}, \sqrt[3]{Q_z^2 J_{max,z}} \right) \tag{54}$$

Similarly, it is known that on the discontinuity, acceleration is at its maximum on $T/2$. The entry feed rates that will be limited by acceleration can then be determined by resolving the following equation:

$$\overrightarrow{A}\left(\frac{T}{2}\right) = \overrightarrow{A_{max,i}} \tag{55}$$

By inserting this condition into equation 35 and using the results given by equations 48 and 49, the following is obtained:

$$V_{lim,a} \quad = \quad \frac{8}{3|\sin\varphi_N\cos\theta_N + \sin\varphi_M\cos\theta_M|} \min\left(\sqrt{Q_x A_{max,x}}, \sqrt{Q_y A_{max,y}}, \sqrt{Q_z A_{max,z}} \right) \tag{56}$$

Thus, maximum acceleration on each of the axes also leads to limitations on the feed rate on entering the block:

$$V_{In} = \min\left(V_F, V_{lim,j}, V_{lim,a}\right) \tag{57}$$

Finally, a last case remains: the transition length calculated L can be greater than the length of the segment upstream or downstream. An additional condition is thus imposed: if $L > ||\overrightarrow{OA}||/2$ or $L > ||\overrightarrow{OB}||/2$, the coordinates of point Q are recalculated taking $L = \min\left(||\overrightarrow{OA}||/2, ||\overrightarrow{OB}||/2\right)$ from equation 52. Equations 54 and 56 then allow the limit feed rate on entry in the discontinuity to be recalculated.

The proposed model is now complete. Experimental validation is proposed in the following section.

4 Experimental validation

Measurements of position profiles, feed rates and acceleration were made on a machine with the aim of validating modelling. Tests were conducted on a DMU 50 eVo 5-axis machining centre equipped with a Siemens 840D Numerical Control. The characteristics of the NC and machine combination are given in table 1. This NC allows measurements of position, feed rate and acceleration to be made for a maximum period of 10 seconds.

Table 1: Characteristics DMU 50 eVo - Siemens 840 D

Dynamic characteristics of axes	
Maximum feed rate	$V_{max,i} = 50 \ m/min$
Maximum acceleration	$A_{max,i} = 9,8 \ m/s^2$
Maximum jerk in translation	$J_{max,i} = 40 \ m/s^3$
Maximum jerk on passage of	$Jc_{max} = 60 \ m/s^3$
a discontinuity in curvature	
Characteristics of the NC	
Tolerances on the axes	$Tol = 0,01 \ mm$
Interpolation time of NC	$2ms$

A test campaign enabled the proposed models to be validated. In particular, feed rates ranging from 500 to 10000 mm/min and machining tolerances from 0.1 to 0.01 mm on various paths were tested. Moreover, as the NC allowed certain dynamic parameters to be modified, jerk was also subjected to variation. In the present publication, only two tests are presented (figure 6[1]): one test in linear interpolation and a second one in circular interpolation. The first test sought to validate the simulation method adopted as well as the method for passage of discontinuities using polynomials. The second confirmed the modelling of behavioural laws on circular portions. The programmed feed rate was 5000 mm/min on the cases studied.

The cutter - workpiece feed rate profiles measured and simulated were plotted on figure 7. What is immediately striking is the model's faithfulness to the experimental curves.

In linear interpolation, the path time calculated is 4237 ms and the time measured on the machine is 4232 ms *i.e.* an error of less than 0.2%. Error between simulation and measurement reaches a maximum level on drops in feed rate at passages between discontinuities (table 2). Although errors between the rate measured and the rate simulated in the discontinuity can appear to be significant, such error on the drop can be seen to represent less than 1%, the profiles are seen to be closed and error on the time of pass through a discontinuity is low.

Figure 8 shows the plots of positions, feed rates and accelerations in projection on the $\overrightarrow{X}$ axis. An excellent match can be seen between the model and the measurement. Figure 9 represents a zoom onto the zone on crossing the discontinuity between the 600th and 900th milliseconds to pass points $2 - 3 - 4$. Note that on the measurements, the feed rate diminishes on the segment to reach a rate of 281 mm/min.

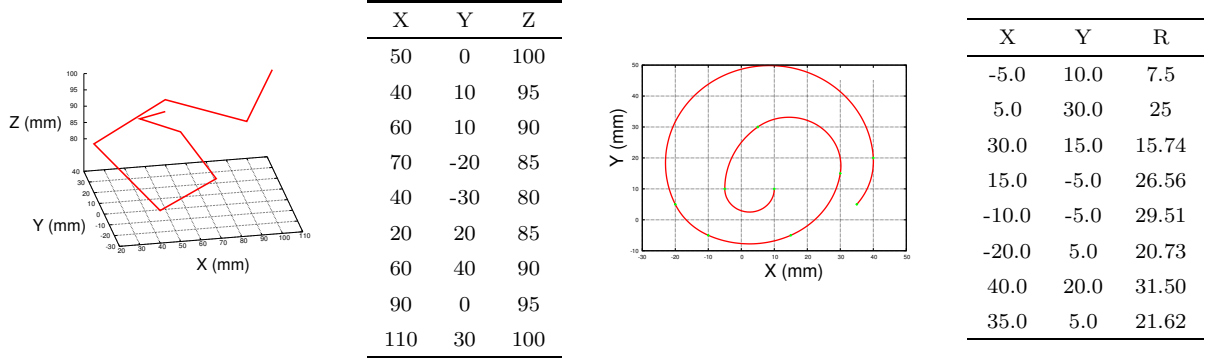[1]In the case of the circular interpolation, X and Y are the coordinates of the final point

X	Y	Z
50	0	100
40	10	95
60	10	90
70	-20	85
40	-30	80
20	20	85
60	40	90
90	0	95
110	30	100

X	Y	R
-5.0	10.0	7.5
5.0	30.0	25
30.0	15.0	15.74
15.0	-5.0	26.56
-10.0	-5.0	29.51
-20.0	5.0	20.73
40.0	20.0	31.50
35.0	5.0	21.62

3-axis paths in linear interpolation   2-axis paths in circular interpolation

Figure 7: Measured and simulated contours for cutter - workpiece feed rates

Linear interpolation

Circular interpolation
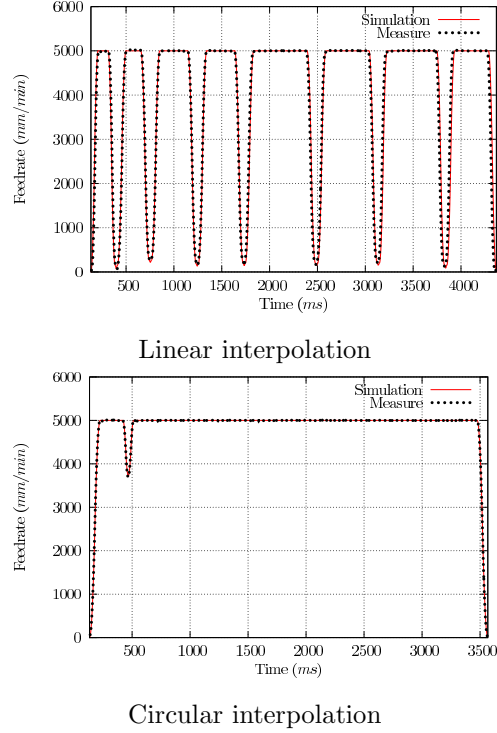
The calculated feed rate is 263 mm/min, representing an error of 6.8%. The discontinuity is then entered. The feed rate measured at the end of the discontinuity is 91 mm/min. The rate calculated is 85 mm/min i.e. 7% of error. Finally, observation of measurement of the acceleration curve shows that there is no leap in acceleration on entering the discontinuity as would tend to suggest passage of a transition by a circle arc. This corroborates the validity of using the model in which acceleration remains continuous.

In circular interpolation, the radius values chosen only highlight a drop in feed rate on passage of the first discontinuity. Error between the calculated value and the simulated value is here only 2%. Error on the difference between the total simulated time and the total calculated time is here also less than 1%.

Table 2: Errors calculated on the cutter - workpiece feed rate on passages of discontinuities (Feed rate in *mm/min*)

	Feed rate in the transition			Drop in feed rate		
	Measurement	Simulation	Error	Measurement	Simulation	Error
1	71	72	1,4 %	4929	4928	0,02 %
2	256	222	13,28 %	4744	4778	0,7 %
3	150	135	10,67 %	4850	4865	0,31 %
4	193	148	23,31 %	4807	4852	0,94 %
5	161	150	6,83 %	4839	4850	0,23 %
6	196	158	19,39 %	4804	4842	0,79 %
7	126	91	27,78 %	4874	4909	0,72 %

Figure 10 shows positions, feed rates and accelerations measured and simulated on the spiral programmed in circular interpolation, in projection on the $\overrightarrow{X}$ axis. The acceleration profile perfectly illustrates the leaps on passage of discontinuities in curvature. The Pateloup model used for simulation is thus fully confirmed.

Figure 11 represents a zoom on a passage through discontinuity. The model can be seen to faithfully reflect the measurement.

5   Conclusion

The present publication proposes a model allowing jumps of discontinuity in tangency to be overcome together with a model to simulate the axial behaviour of a machine in circular interpolation. This means that the position, feed rate, acceleration and jerk on each of the axes catering for the dynamic parameters of the machine/NC combinations can be simulated on 3 axes and cutter - workpiece contours be determined. This gives faithful simulation of the machine's dynamic behaviour in 3-axis machining in the commonest programming modes.

Moreover, the present study stresses the problem of using linear interpolation when finishing complex workpieces. In this context, programmed tolerances are often extremely low and segments thus extremely short, leading to repeated reductions in feed rate. This problem is only very partially resolved by NCs using predictive functions.

This means that beyond a certain segment size, the type of programming needs to be changed. Future works will therefore study the machine dynamics in polynomial interpolation and integration of this type of programming into the simulator. The possibility of integrating the behaviour of series 5-axis machines into the model can then be considered. Finally, in the longer term, the simulator should allow for machining paths to be optimized so as to boost the productivity of ultra-high speed machines.

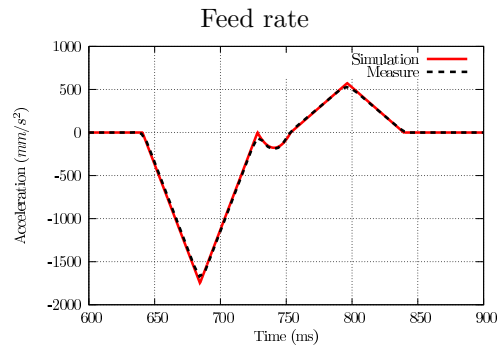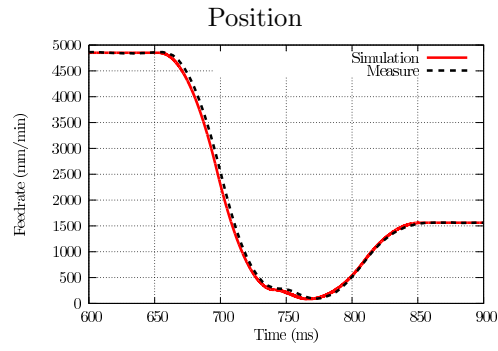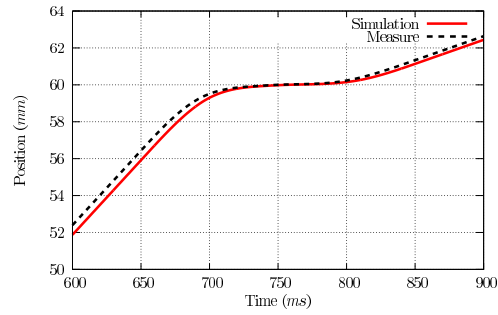Figure 8: Comparison of contours measured and simulated on a rectilinear path
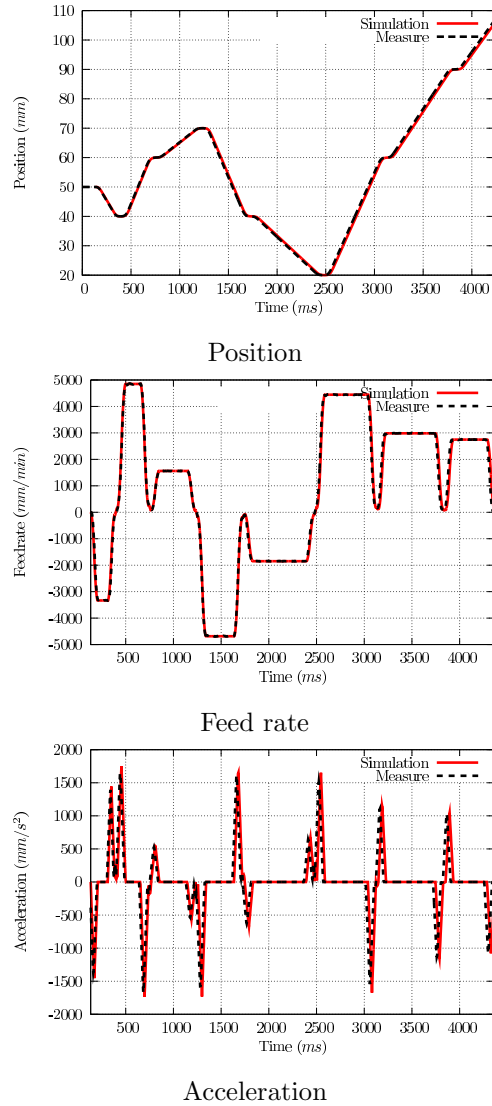
Position

Feed rate

Acceleration

Acknowledgements

21

Figure 9: Passage of a discontinuity at a tangent

Position

Feed rate

Acceleration

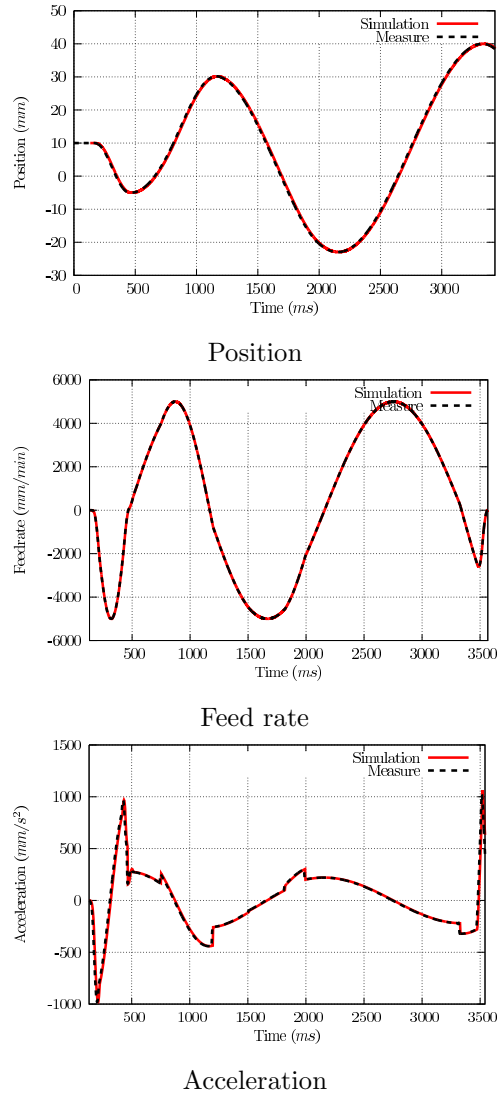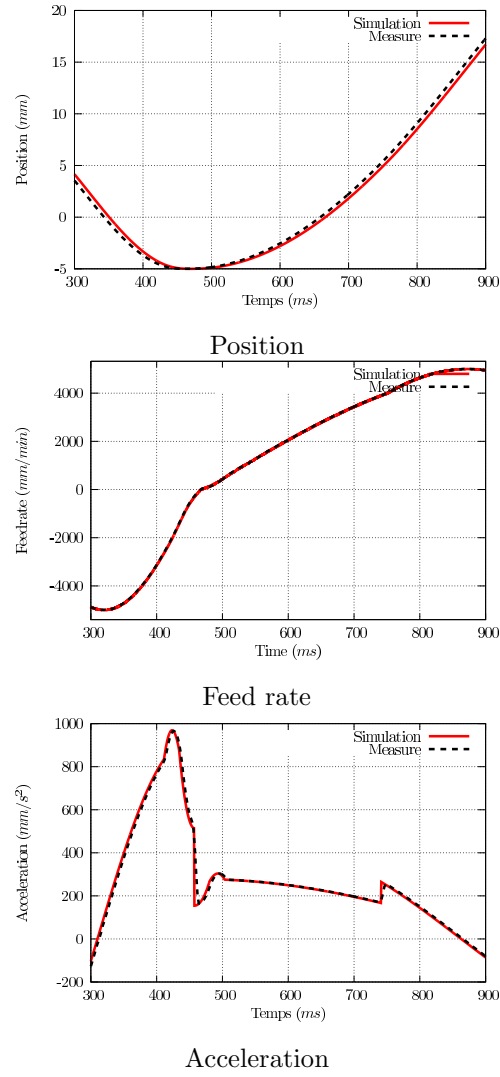Figure 10: Comparison of contours measured and simulated on the circular path

Position

Feed rate

Acceleration

23

Figure 11: Passage of a discontinuity in a curvature

Position

Feed rate

Acceleration

References

[1] Tapie, L., Mawussi, K. & Anselmetti, B., Circular tests for HSM machine tools: Bore machining application, International Journal of Machine Tools and Manufacture , 47(5), 805-819 (2007).

[2] Flores, V., Ortega, C., Alberti, M., Rodriguez, C A, de Ciurana, J. & Elias, A., Evaluation and modeling of productivity and dynamic capability in high-speed machining centers, The International Journal of Advanced Manufacturing Technology, 33(3), 403-411 (2007).

[3] Korkut, I. & Donertas, M., The influence of feed rate and cutting speed on the cutting forces, surface roughness and tool-chip contact length during face milling, Materials & Design , 28(1), 308-312 (2007).

[4] Tsai, M.-., Cheng, C.-. & Cheng, M.-., A real-time NURBS surface interpolator for precision three-axis CNC machining, International Journal of Machine Tools and Manufacture , 43(12), 1217-1227 (2003).

[5] Liu, X. et al., Adaptive interpolation scheme for NURBS curves with the integration of machining dynamics, International Journal of Machine Tools and Manufacture , 45(4-5), 433-444 (2005).

[6] Xu, R. Z., Xie,L. , Li, C. X., & Du, D. S., Adaptive parametric interpolation scheme with limited acceleration and jerk values for NC machining, The International Journal of Advanced Manufacturing Technology , 36(3), 343-354 (2008).

[7] Sencer, B. & Altintas, Y., Feed optimization for five-axis CNC machine tools with drive constraints, International Journal of Machine Tools and Manufacture , 48(7-8), 733-745 (2008).

[8] Siemens, `http://www.automation.siemens.com/doconweb`.

[9] Erkorkmaz, K. & Altintas, Y., High speed CNC system design. Part I: jerk limited trajectory generation and quintic spline interpolation, International Journal of Machine Tools and Manufacture, 41(9), 1323-1345 (2001).

[10] Aguilar, I. H., Commande des bras manipulateurs et retour visuel pour des applications à la robotique de service, PhD Thesis, Université de Toulouse III (2006).

[11] Nam, S. & Yang, M., A study on a generalized parametric interpolator with real-time jerk-limited acceleration, Computer-Aided Design , 36(1), 27-36 (2004).

[12] Lavernhe, S., Tournier, C. & Lartigue, C., Kinematical performance prediction in multi-axis machining for process planning optimization. The International Journal of Advanced Manufacturing Technology , 37(5), 534-544 (2008).

[13] Tounsi, N., Bailey, T. & Elbestawi, M.A., Identification of acceleration deceleration profile of feed drive systems in CNC machines, International Journal of Machine Tools and Manufacture , 43(5), 441-451 (2003).

[14] Manuel & A, C., Influence of tool path strategy on the cycle time of high-speed milling, Computer-Aided Design , 35(4), 395-401 (2003).

[15] Pateloup, V., Duc, E. & Ray, P., Corner optimization for pocket machining, International Journal of Machine Tools and Manufacture, 44(12-13), 1343-1353 (2004).

Appendices: General case for the path of a uniaxial segment

The non-linear system described in section 1 therefore needs to be resolved. This resolution involves resolving the 10 cases shown in figure 3.

The assumption is made that acceleration is null on entry and exit of the block. This is verified when the segments are long enough to reach the feed rate programmed at the end of the segment (section 3.5).

Resolution of this system means the times for each of the phases can be determined so as to plot the cutter - workpiece feed rate profile. In some cases, the programmed feed rate will not be reached and the rate actually reached will be sought.

According to the distance to be covered and the jumps in feed rate to be crossed, 10 cases were listed. From resolution of equations 1 to 7, the following obtains:

- Case 1: V_{Out} cannot be reached. V'_{Out} is reached by reaching $A_{max,i}$ (figure 12):

$$
\begin{cases}
|V_{Out} - V_{In}| \geq \frac{A^2_{max,i}}{J_{max,i}} \\
2V_{In}\frac{A_{max,i}}{J_{max,i}} + \frac{A^3_{max,i}}{J^2_{max,i}} \leq L \leq \\
\quad \frac{J_{max,i}(V^2_{Out}-V^2_{In})+A^2_{max,i}(V_{In}+V_{Out})}{2A_{max,i}J_{max,i}}
\end{cases}
\tag{58}
$$

$$
\begin{aligned}
V'_{Out} \quad = \quad & \frac{1}{2J_{max,i}} \\
& \cdot \Big(A_{max,i}J^2_{max,i}L + 4J^2_{max,i}V^2_{In} \\
& -4A^2_{max,i}J_{max,i}V_{In} + A^4_{max,i}\Big)^{1/2} \\
& -A^2_{max,i}
\end{aligned}
\tag{59}
$$

$$
\begin{cases}
\tau_1 = \tau_3 = \frac{A_{max,i}}{J_{max,i}} \\
\tau_2 = \frac{V'_{Out}-V_{In}}{A_{max,i}} - \frac{A_{max,i}}{J_{max,i}} \\
\tau_4 = \tau_5 = \tau_6 = \tau_7 = 0
\end{cases}
\tag{60}
$$

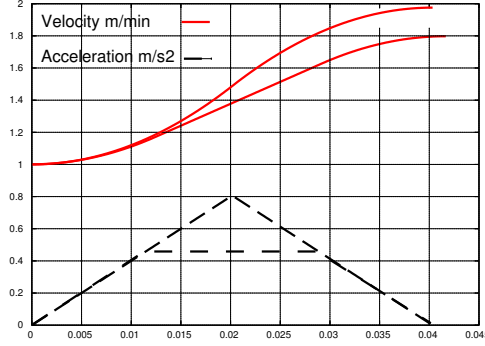- Case 2: V_{Out} cannot be reached. V'_{Out} is reached without reaching $A_{max,i}$ (figure 12):

$$
\begin{cases}
|V_{Out} - V_{In}| \geq \frac{A^2_{max,i}}{J_{max,i}} \\
L \leq 2V_{In}\frac{A_{max,i}}{J_{max,i}} + \frac{A^3_{max,i}}{J^2_{max,i}}
\end{cases}
\tag{61}
$$

$$
\begin{cases}
|V_{Out} - V_{In}| \leq \frac{A^2_{max,i}}{J_{max,i}} \\
L \leq (V_{Out} + V_{In})\sqrt{\frac{V_{Out}-V_{In}}{J_{max}}}
\end{cases}
\tag{62}
$$

$$
V'_{Out} = V_{In} + J_{max,i}\tau_1^2
\tag{63}
$$

$$
\begin{cases}
\tau_1 \text{ is solution of } J_{max,i}\tau_1^3 + 2V_{In}\tau_1 - L = 0 \\
\tau_1 = \tau_3 \\
\tau_2 = \tau_4 = \tau_5 = \tau_6 = \tau_7 = 0
\end{cases}
\tag{64}
$$

Figure 12: Cases 1 and 2

- Case 3: V_{Out} is reached by reaching $A_{max,i}$. V_F is not reached. V'_F is reached by reaching $A_{max,i}$. $\tau_1 = \tau_3 = \tau_5 = \tau_7 = A_{max,i}/J_{max,i}$ V'_F, τ_1 and τ_6 are solutions of:

$$
\begin{cases}
V'_F &= \frac{A^2_{max,i}}{J_{max,i}} + V_{In} + A_{max,i}\tau_2 \\
V_{Out} &= -\frac{A^2_{max}}{J_{max,i}} + V'_F - A_{max,i}\tau_6 \\
L &= \frac{1}{2J_{max,i}} \cdot \\
& \quad \Big(\big(2\tau_2 V_{In} + 2\tau_6 V'_F - A_{max,i}\tau_6^2 \\
& \quad + A_{max,i}\tau_2^2 \big) \cdot J_{max,i} \\
& \quad + 4A_{max,i}V_{In} + 4A_{max,i}V'_F \\
& \quad - 3A^2_{max,i}\tau_6 + 3A^2_{max,i}\tau_2 \Big)
\end{cases}
\tag{65}
$$

- Case 4: V_{Out} is reached without reaching $A_{max,i}$. V_F is not reached. V'_F is reached by reaching $A_{max,i}$. $\tau_1 = \tau_3 = A_{max,i}/J_{max,i}$ and V'_F, τ_2, τ_5 are solutions of:

$$
\begin{cases}
V'_F &= \frac{A^2_{max,i}}{J_{max,i}} + V_{In} + A_{max,i}\tau_2 \\
V_{Out} &= V'_F - \tau_5^2 J_{max,i} \\
L &= -\tau_5^3 J_{max,i} + \frac{2A_{max}V_{In}}{J_{max,i}} \\
& \quad + \frac{3A^2_{max,i}\tau_2}{2J_{max,i}} + \frac{A^3_{max,i}}{J^2_{max,i}} \\
& \quad + \tau_2 V_{In} + 2\tau_5 V'_F + \frac{A_{max,i}\tau_2^2}{2}
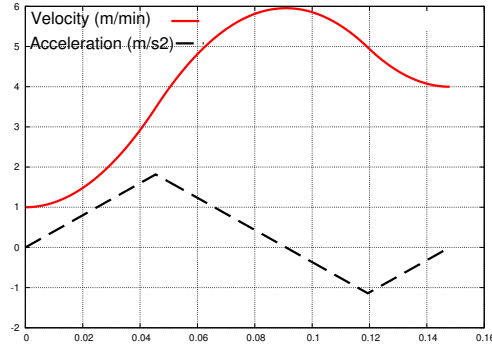\end{cases}
\tag{66}
$$

- Case 5: V_{Out} is reached by reaching $A_{max,i}$. V_F is not reached. V'_F is reached without reaching $A_{max,i}$. $\tau_5 = \tau_7 = A_{max,i}/J_{max,i}$, $\tau_2 = 0$, $\tau_1 = \tau_3$, τ_1, τ_6 and V'_F are solutions of:

$$
\begin{cases}
V'_F &= V_{In} + J_{max,i}\tau_1^2 \\
V_{Out} &= -\frac{A^2_{max,i}}{J_{max,i}} + V'_F - A_{max,i}\tau_6 \\
L &= \frac{1}{2J^2_{max,i}} \cdot \\
& \quad \Big(2\tau_1^3 J^3_{max,i} \\
& \quad + (4\tau_1 V_{In} + 2\tau_6 V'_F - A_{max,i}\tau_6^2)J^2_{max,i} \\
& \quad + (4A_{max,i}Vc - 3A^2_{max,i}\tau_6)J_{max,i} \\
& \quad - 2A^3_{max,i} \Big)
\end{cases}
\tag{67}
$$

27

- Case 6: V_{Out} is reached without reaching $A_{max,i}$. V_F is not reached. V_F' is reached without reaching $A_{max,i}$. $\tau_1 = \tau_3$, $\tau_5 = \tau_7$, τ_1, τ_5 and V_F' are solutions of (figure 13) :

$$
\begin{cases}
V_F' = \tau_1^3 J_{max,i} + 2\tau_1 V_{In} \\
V_{Out} = V_F' - \tau_7^2 J_{max,i} \\
L = -\tau_7^3 J_{max,i} + \tau_1^3 J_{max,i} + 2\tau_1 V_{In} + 2\tau_7 V_F'
\end{cases}
\tag{68}
$$

Figure 13: Case 6

- Case 7: V_{Out} is reached by reaching $A_{max,i}$. V_F is reached. V_F is reached by reaching $A_{max,i}$.

$$
\begin{cases}
|V_F - V_{In}| \geq \frac{A_{max,i}^2}{J_{max,i}} \\
|V_{Out} - V_F| \geq \frac{A_{max,i}^2}{J_{max,i}} \\
L \geq \frac{1}{2A_{max,i}J_{max,i}} \cdot \\
\quad \Big(\left(2J_{max,i}V_F + 2A_{max,i}^2\right)V_{In} \\
\quad + J_{max,i}V_F^2 + A_{max,i}^2 V_F \\
\quad + \left(2J_{max,i}V_{Out} + 2A_{max,i}^2\right)V_F \\
\quad + J_{max,i}V_{Out}^2 + A_{max,i}^2 V_{Out} \Big)
\end{cases}
\tag{69}
$$

$$
\begin{cases}
\tau_1 = \tau_3 = \tau_5 = \tau_7 = \frac{A_{max}}{J_{max}} \\
\tau_2 = \frac{V_F}{A_{max}} - \frac{A_{max}}{J_{max}} \\
\tau_6 = \frac{V_{Out}}{A_{max}} - \frac{A_{max}}{J_{max}}
\end{cases}
\tag{70}
$$

- Case 8: V_{Out} is reached without reaching $A_{max,i}$. V_F is reached. V_F is reached by reaching $A_{max,i}$.

$$
\begin{cases}
|V_F - V_{In}| \geq \frac{A_{max,i}^2}{J_{max,i}} \\
|V_{Out} - V_F| \leq \frac{A_{max,i}^2}{J_{max,i}} \\
L \geq \frac{\left(2J_{max,i}V_F + 2A_{max,i}^2\right)V_{In} + J_{max,i}V_F^2 + A_{max,i}^2 V_F}{2A_{max,i}J_{max,i}} \\
\quad + \frac{\sqrt{J_{max}V_{Out}}(4V_F + V_{Out}) + A_{max}V_F}{2J_{max}}
\end{cases}
\tag{71}
$$

$$
\begin{cases}
\tau_1 = \tau_3 = \frac{A_{max,i}}{J_{max,i}} \\
\tau_2 = \frac{V_F - V_{In}}{A_{max,i}} - \frac{A_{max,i}}{J_{max,i}} \\
\tau_5 = \tau_7 = \sqrt{\frac{V_F - V_{Out}}{J_{max,i}}} \\
\tau_6 = 0
\end{cases}
\tag{72}
$$

28

- Case 9: V_{Out} is reached by reaching $A_{max,i}$. V_F is reached. V_F is reached without reaching $A_{max,i}$.

$$\begin{cases} |V_F - V_{In}| \le \frac{A_{max,i}^2}{J_{max,i}} \\ |V_{Out} - V_F| \ge \frac{A_{max,i}^2}{J_{max,i}} \\ L \ge \frac{\sqrt{J_{max}V_F(4V_{In}+V_F)}+A_{max}V_{In}}{2J_{max}} \\ \qquad + \frac{\left(2J_{max,i}V_{Out}+2A_{max,i}^2\right)V_F + J_{max,i}V_{Out}^2 + A_{max,i}^2V_{Out}}{2A_{max,i}J_{max,i}} \end{cases} \tag{73}$$
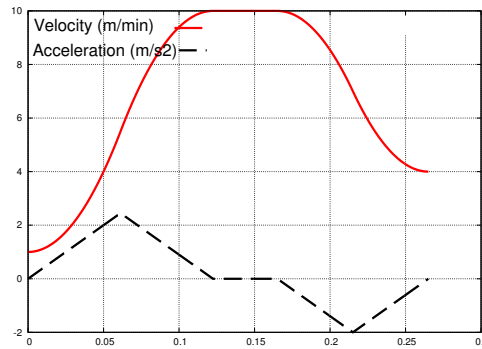
$$\begin{cases} \tau_1 = \tau_3 = \sqrt{\frac{V_{In}-V_F}{J_{max,i}}} \\ \tau_2 = 0 \\ \tau_5 = \tau_7 = \frac{A_{max,i}}{J_{max,i}} \\ \tau_6 = \frac{V_{Out}-V_F}{A_{max,i}} - \frac{A_{max,i}}{J_{max,i}} \end{cases} \tag{74}$$

- Case 10: V_{Out} is reached without reaching $A_{max,i}$. V_F is reached. V_F is reached without reaching $A_{max,i}$ (figure 14) :

$$\begin{cases} |V_F - V_{In}| \le \frac{A_{max,i}^2}{J_{max,i}} \\ |V_{Out} - V_F| \le \frac{A_{max,i}^2}{J_{max,i}} \\ L \ge \frac{\sqrt{J_{max}V_F(4V_{In}+V_F)}+A_{max}V_{In}}{2J_{max}} \\ \qquad + \frac{\sqrt{J_{max}V_{Out}(4V_F+V_{Out})}+A_{max}V_F}{2J_{max}} \end{cases} \tag{75}$$

$$\begin{cases} \tau_1 = \tau_3 = \sqrt{\frac{V_{In}-V_F}{J_{max,i}}} \\ \tau_2 = 0 \\ \tau_5 = \tau_7 = \sqrt{\frac{V_F-V_{Out}}{J_{max,i}}} \\ \tau_6 = 0 \end{cases} \tag{76}$$

Figure 14: Case 10

In the simulations, equation 2 is resolved by the Cardan method. The systems of equation 65, 66, 67 and 68 are non-linear. They are resolved numerically using the Newton-Raphson method.

To use this algorithm, take a segment of $0.01m$ to be covered. Take $V_{In} = 0.2m/s$, $V_{Out} = 0.1m/s$, $V_F = 0.5m/s$. The machine parameters are those in table 1.

$|V_{Out} - V_{In}| \le \frac{A_{max,i}^2}{J_{max,i}}$; thus there will be no phase 2. $L \ge (V_{Out} + V_{In})\sqrt{\frac{V_{Out}-V_{In}}{J_{max}}}$; the length of the segment thus allows V_{Out} to be reached.

$|V_F - V_{In}| \leq \frac{A_{max,i}^2}{J_{max,i}}$ and $|V_{Out} - V_F| \leq \frac{A_{max,i}^2}{J_{max,i}}$ and $L \leq \frac{\sqrt{J_{max}V_{Out}}(4V_F+V_{Out})+A_{max}V_F}{2J_{max}}$. The length does therefore not allow V_F to be reached and the differences in feed rates will not allow maximum acceleration to be reached. This means case 6 applies. This gives$V_F' = 0.4418m/s$,

$$\tau_1 = \tau_3 = 0.07776s. \quad \tau_5 = \tau_7 = 0.09245s.$$